星形成ゼミ

37. # Imaging of HH80-81 jet in the NIR shock tracers H_2 and [Fe II]

Sreelekshmi Mohan, Sarita Vig, Watson P. Varricatt, Anandmayee Tej ★ The HH80-81 system is one of the most powerful jets driven by a massive protostar. We present new near-infrared (NIR) line imaging observations of the HH80-81 jet in the H_2 (2.122 μm) and [Fe II] (1.644 μm) lines. These lines trace not only the jet close to the exciting source but also the knots located farther away. We have detected nine groups of knot-like structures in the jet including HH80 and HH81 spaced $0.2 - 0.9$ pc apart. The knots in the northern arm of the jet show only [Fe II] emission closer to the exciting source, a combination of [Fe II] and H_2 at intermediate distances, and solely H_2 emission farther outwards. Towards the southern arm, all the knots exhibit both H_2 and [Fe II] emission. The nature of the shocks is inferred by assimilating the NIR observations with radio and X-ray observations from literature. In the northern arm, we infer the presence of strong dissociative shocks, in the knots located close to the exciting source. The knots in the southern arm that include HH80 and HH81 are explicable as a combination of strong and weak shocks. The mass-loss rates of the knots determined from [Fe II] luminosities are in the range $\sim 3.0 \times 10^{-7} - 5.2 \times 10^{-5}$ $M_\odot$ yr^{-1}, consistent with those from massive protostars. Towards the central region, close to the driving source of the jet, we have observed various arcs in H_2 emission which resemble bow shocks, and strings of H_2 knots which reveal traces of multiple outflows.

38. The complex organic molecular content in the L1517B starless core

Andrés Megías, Izaskun Jiménez-Serra, Jesús Martín-Pintado, Anton I. Vasyunin, Silvia Spezzano, Paola Caselli, Giuliana Cosentino, Serena Viti

★ Recent observations of the pre-stellar core L1544 and the younger starless core L1498 have revealed that complex organic molecules (COMs) are enhanced in the gas phase toward their outer and intermediate-density shells. Our goal is to determine the level of chemical complexity toward the starless core L1517B, which seems younger than L1498, and compare it with the other two previously studied cores to see if there is a chemical evolution within the cores. We have carried out 3 mm high-sensitivity observations toward two positions in the L1517B starless core: the core's centre and the position where the methanol emission peaks (at a distance of ∼5000 au from the core's centre). Our observations reveal that a lower number of COMs and COM precursors are detected in L1517B with respect to L1498 and L1544, and also show lower abundances. Besides methanol, we only detected H_2CCO, CH_3CHO, CH_3CN, CH_3NC, HCCCN, and HCCNC. Their measured abundances are ∼3 times larger toward the methanol peak than toward the core's centre, mimicking the behaviour found toward the more evolved cores L1544 and L1498. We propose that the differences in the chemical complexity observed between the three studied starless cores are a consequence of their evolution, with L1517B being the less evolved one, followed by L1498 and L1544. Chemical complexity in these cores seems to increase over time, with N-bearing molecules forming first and O-bearing COMs forming at a later stage as a result of the catastrophic depletion of CO.

39. # Importance of source structure on complex organics emission III. Effect of disks around massive protostars

P. Nazari, B. Tabone, G. P. Rosotti ★ Complex organic molecules are only detected toward a fraction of high-mass protostars. The goal of this work is to investigate whether high-mass disks can explain the lack of methanol emission from some massive protostellar systems. We consider an envelope-only and an envelope-plus-disk model and use RADMC-3D to calculate the methanol emission. High and low millimeter (mm) opacity dust are considered for both models separately and the methanol abundance is parameterized. Viscous heating is included due to the high accretion rates of these objects in the disk. In contrast with low-mass protostars, the presence of a disk does not significantly affect the temperature structure and methanol emission. The shadowing effect of the disk is not as important for high-mass objects and the disk mid-plane is hot because of viscous heating, which is effective due to the high accretion rates. Consistent with observations of infrared absorption lines toward high-mass protostars, we find a vertical temperature inversion, i.e. higher temperatures in the disk mid-plane than the disk surface, at radii $<$ 50au for the models with $L = 10^4$ $L_\odot$ and large mm opacity dust as long as the envelope mass is $>$550 $M_\odot$. The large observed scatter in methanol emission from massive protostars can be mostly explained toward lower luminosity objects with the envelope-plus-disk models including low and high mm opacity dust. The methanol emission variation toward sources with high luminosities cannot be explained by models with or without a disk. However, the L/M of these objects suggest that they could be associated with hypercompact/ultracompact HII regions. Therefore, the low methanol emission toward the high-luminosity sources can be explained by them hosting an HII region where methanol is absent.

40. Turbulence, Coherence and Collapse: Three Phases for Core Evolution

Stella S. R. Offner, Josh Taylor, Carleen Markey, Hope How-Huan Chen, Jaime E. Pineda, Alyssa A. Goodman, Andreas Burkert, Adam Ginsburg, Spandan Choudhury

★ We study the formation, evolution and collapse of dense cores by tracking structures in a magnetohydrodynamic simulation of a star-forming cloud. We identify cores using the dendrogram algorithm and utilize machine learning techniques, including Neural Gas prototype learning and Fuzzy *c*-means clustering, to analyze the density and velocity dispersion profiles of cores together with six bulk properties. We produce a 2-d visualization using a Uniform Manifold Approximation and Projection (UMAP), which facilitates the connection between physical properties and three partially-overlapping phases: i) unbound turbulent structures (Phase I), ii) coherent cores that have low turbulence (Phase II), and iii) bound cores, many of which become protostellar (Phase III). Within Phase II we identify a population of long-lived coherent cores that reach a quasi-equilibrium state. Most prestellar cores form in Phase II and become protostellar after evolving into Phase III. Due to the turbulent cloud environment, the initial core properties do not uniquely predict the eventual evolution, i.e., core evolution is stochastic, and cores follow no one evolutionary path. The phase lifetimes are $1.0\pm0.1\times10^5$ yr, $1.3\pm0.2\times10^5$ yr, and $1.8\pm0.3\times10^5$ yr for Phase I, II, and III, respectively. We compare our results to NH_3 observations of dense cores. Known coherent cores predominantly map into Phase II, while most turbulent pressure-confined cores map to Phase I or III. We predict that a significant fraction of observed starless cores have unresolved coherent regions and that $\gtrsim 20\%$ of observed starless cores will not form stars. Measurements of core radial profiles, in addition to the usual bulk properties, will enable more accurate predictions of core evolution.

背景

- 観測
  - Coherent core (line widthがsubsonicになり、Bonnor-Ebert球の分布とよく似た密度分布 e.g., Goodman+ 1998, Lada & Lada 2001)
  - Droplets (重力ではなく外圧により束縛された小質量コア。Ophiuchus and Taurus。BE球より緩やかな密度分布 Chen+2019ab)
- この論文の目的
  - Coherent coreには、重力的に束縛されたコアから、外圧により束縛されたコアまで様々な種類がある。
  - これのcoherent coresの間の関係、またcoherent coreとpre-/protostellar coreの間の関係を知りたい。
  - MHDシミュレーションでコアを追跡して、コアの物理状態の進化を調べる。

- MHD計算設定
  - (5 pc)^3 with periodic bound.
  - Mean density ~ 430 /cc
  - Uniform Bz 13.5uG
  - $1 \leq \frac{kL}{2\pi} \leq 2$ で乱流を注入して定常状態にする
    - Virial parameter ~ 1
    - $\beta \sim 0.02$

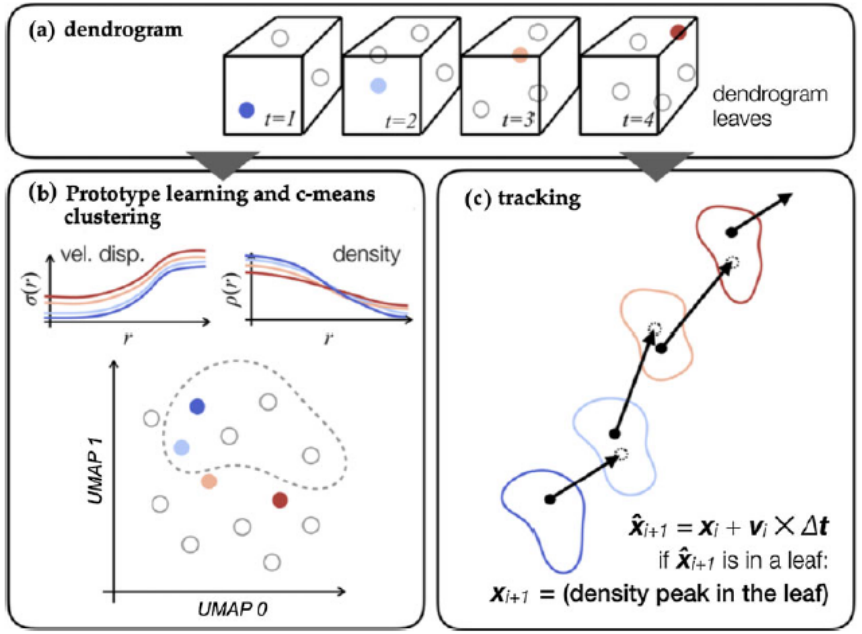

コア同定と追跡

- Dendrogram (Rosolwsky+2008)
  - >10^4 /ccの領域
  - 速度から予想される位置とコアを比較して追跡
  - 6x10^5 yrの間に3538structureを同定
    - 450 tracks。このうち146が、ほかのtackと合体して、もはや一つの構造と同定できなくなる。
      → 今回はこのようなコアは省く

コアを特徴づける量→機械学習
→ 似た性質を持つグループの同定

- コアの動径分布
  - 複数の密度値n_i(51個)で等値面を書き、
    これを球としたときの半径$R_{\mathrm{eq},i}$を求める。
  - $n(r)$はn_iと$R_{\mathrm{eq},i}$から求める
  - 同様に速度分散の動径分布も求める
- 特徴づける量 (d=106次元)
  - 密度分布のFWHM R_{c}
  - 質量 $M_{\mathrm{c}} = M(R < R_{\mathrm{c}})$
  - 速度分散 $\sigma_{\mathrm{c}} = \sigma(R_{\mathrm{c}})/\sqrt{3}$
  - Radius of coherence R_{coh}
    $\frac{\sigma_{\mathrm{c}}}{\sqrt{3}} < c_{\mathrm{s}}$を満たす半径
  - 運動エネルギー $3M_{\mathrm{c}}\sigma_{\mathrm{tot}}^2/2$
  - 重力エネルギー $-3GM_{\mathrm{c}}/(5R_{\mathrm{c}})$

Fuzzy c-means clustering で同定したグループを
UMAPというものを使って二次元に可視化

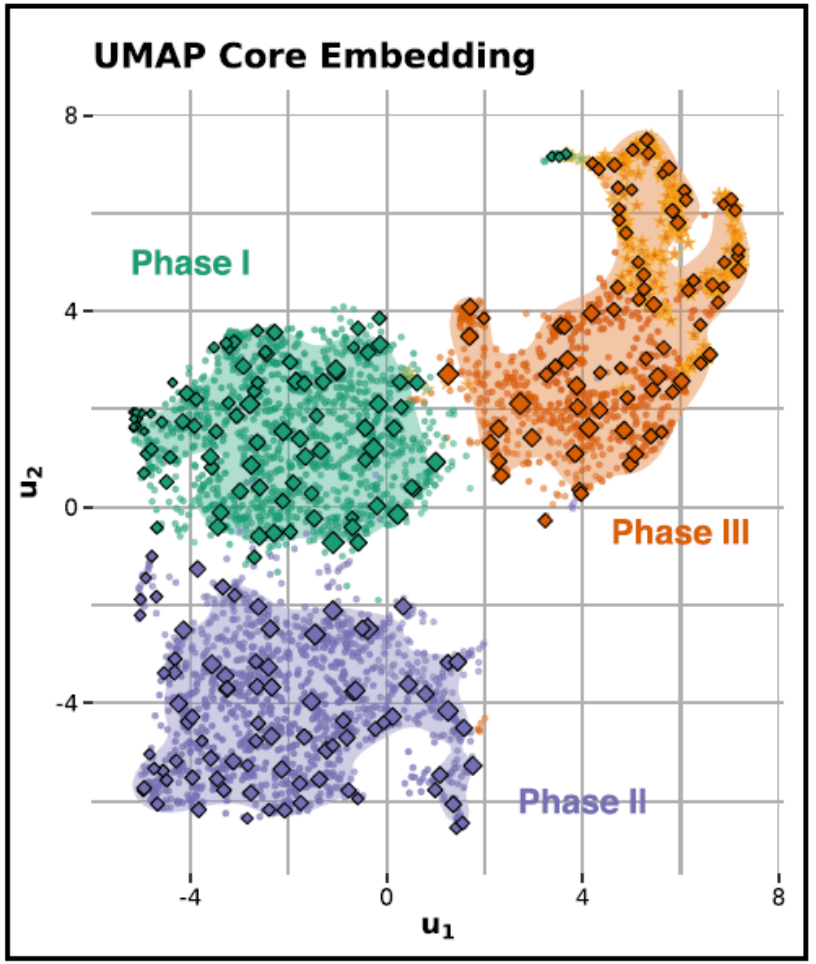

Table 1. Physical properties of cores in each phase. We assign those that have partial membership in two different clusters to the one with the highest membership. The physical properties are measured using the density and velocity profiles derived from the dendrogram structure. The columns are number of cores and median core mass, radius, size of the coherent region, density index, total velocity dispersion, bulk velocity, ratio between the kinetic energy, and the absolute value of the gravitational potential energy, fraction of members containing protostars, and nearest neighbour separation. The density index is the power-law index of the function, $n = n_0 (r/r_0)^p$, fitted to the density profile of each core. The spreads are calculated using the 0.25 and 0.75 quantiles of the distribution.

Core classification	N	M_c ($M_\odot$)	R_c (pc)	R_{coh} (pc)	p	σ_{tot} (km s^{-1})	$V_{bulk,\,1d}$ (km s^{-1})	$\Omega_K/\lvert\Omega_G\rvert$	f_* (%)	$\bar{d}$ (pc)
Phase I (turbulent)	1221	$0.3^{+0.2}_{-0.1}$	$0.034^{+0.008}_{-0.008}$	$0.012^{+0.004}_{-0.004}$	$-0.9^{+0.2}_{-0.2}$	$0.27^{+0.03}_{-0.02}$	$0.6^{+0.2}_{-0.2}$	$6.3^{+3.1}_{-1.6}$	0.82	$0.17^{+0.11}_{-0.07}$
Phase II (coherent)	1317	$0.4^{+0.2}_{-0.1}$	$0.040^{+0.007}_{-0.008}$	$0.029^{+0.009}_{-0.006}$	$-0.9^{+0.1}_{-0.2}$	$0.23^{+0.02}_{-0.01}$	$0.4^{+0.3}_{-0.2}$	$3.2^{+0.9}_{-0.6}$	0.0	$0.18^{+0.13}_{-0.07}$
Phase III (protostellar)	1000	$0.3^{+0.2}_{-0.2}$	$0.023^{+0.006}_{-0.004}$	$0.008^{+0.007}_{-0.008}$	$-1.2^{+0.2}_{-0.3}$	$0.26^{+0.04}_{-0.02}$	$0.6^{+0.2}_{-0.2}$	$2.9^{+1.6}_{-1.0}$	22.9	$0.13^{+0.06}_{-0.05}$
All	3538	$0.3^{+0.2}_{-0.1}$	$0.032^{+0.01}_{-0.008}$	$0.016^{+0.01}_{-0.007}$	$-0.9^{+0.2}_{-0.3}$	$0.25^{+0.03}_{-0.02}$	$0.5^{+0.3}_{-0.2}$	$3.9^{+2.1}_{-1.1}$	6.8	$0.16^{+0.10}_{-0.06}$

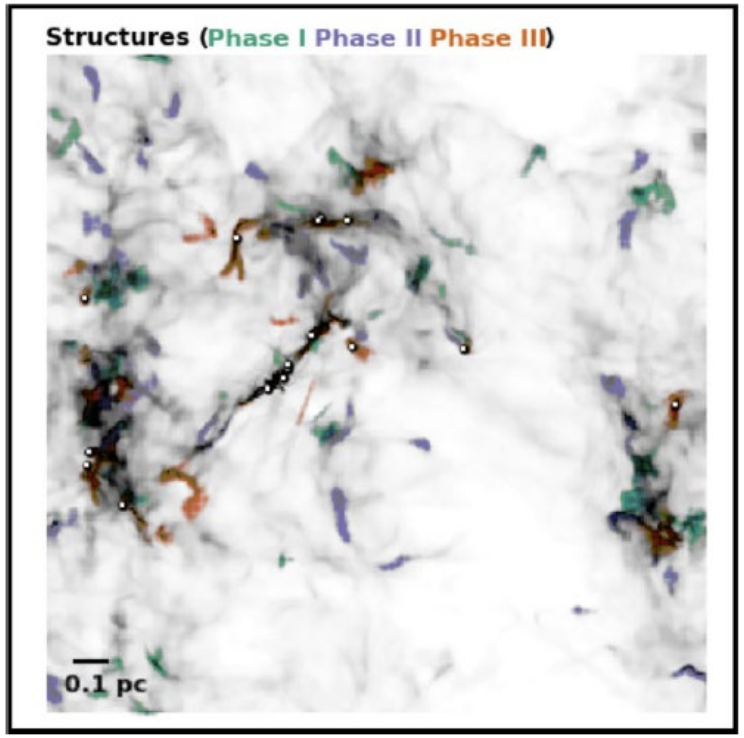

- Phase III → ほとんどは大きなfilamentsに存在
- Phase IとII
  → 多くが衝撃波やより孤立したfilamentに存在

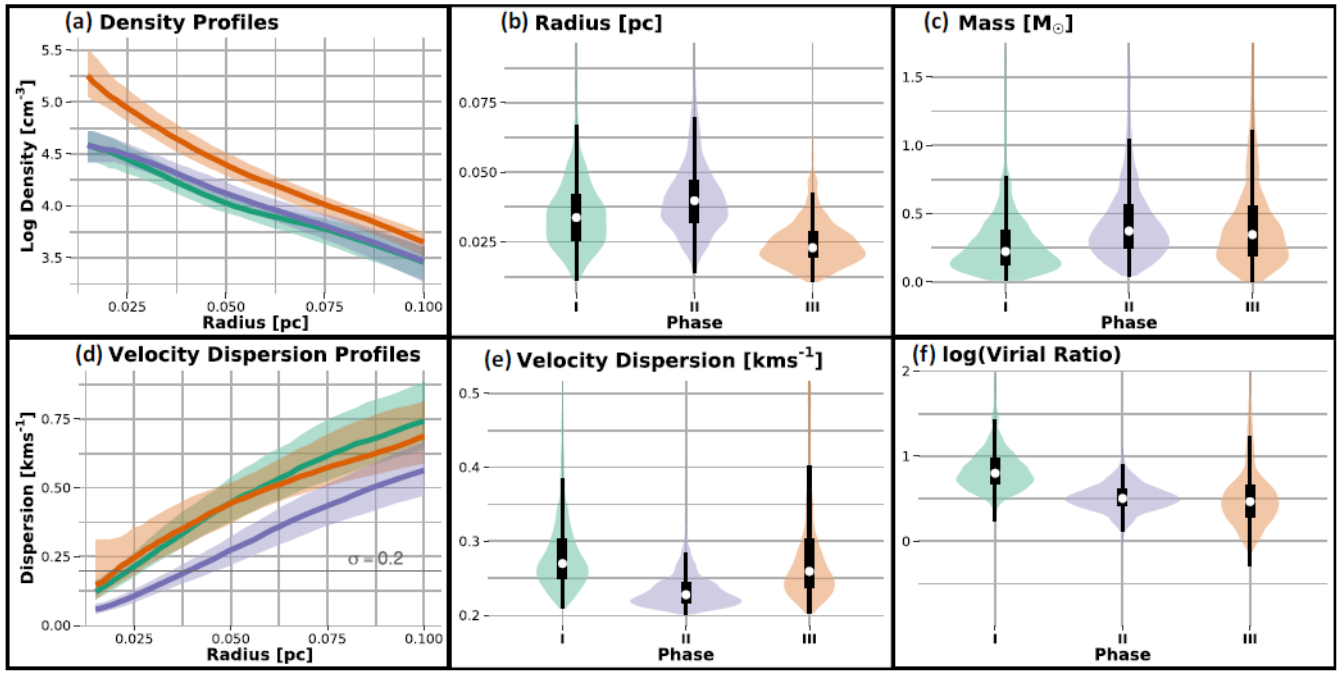

- **密度分布**
  - Phase IとIIには大きな違いがなく、Phase IIIの分布は密度分布はより急峻
- **速度分散分布**
  - 中心に向かって減少する。
  - Phase IとPhase IIIは同じ程度の速度分散。Phase IIだけ中心にsubsonicなcoherent領域が存在

コアの進化

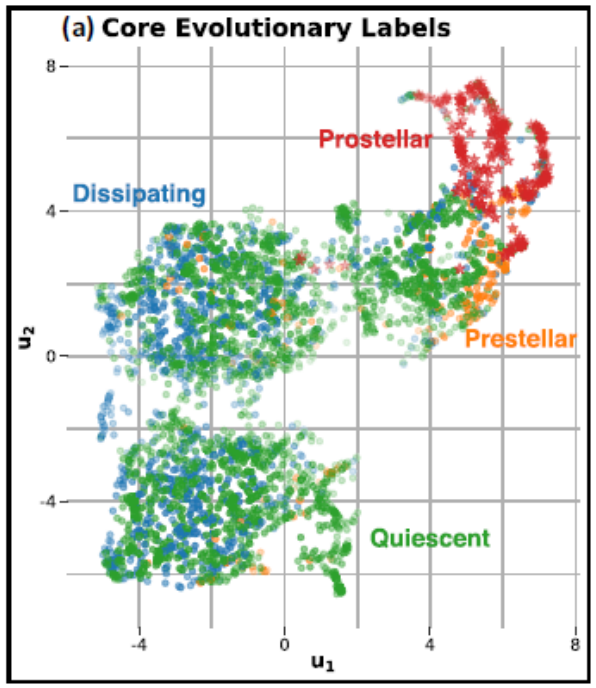

赤：Protostellar
オレンジ：prestellar
緑：quiescent
青：dissipating

コア進化は動的
- 85%は少なくとも一回phaseが変化するか、散逸する
- 瞬間瞬間の性質でその後の進化が決まるわけではない

一般的な傾向
- Short-lived→ Phase IかPhase II
- Long-lived → Phase I, II, IIIにある
- Protostarを生むコア
  → 生まれるときは3つのphaseどれでもあり得るが、Phase IIIで最も長い時間を過ごす。

- 平均寿命
  - Phase I → $1.0 \pm 0.1 \times 10^5$ yr
  - Phase II→ $1.3 \pm 0.2 \times 10^5$yr
  - Phase III → $1.8 \pm 0.3 \times 10^5$ yr

Phase間の遷移の確率

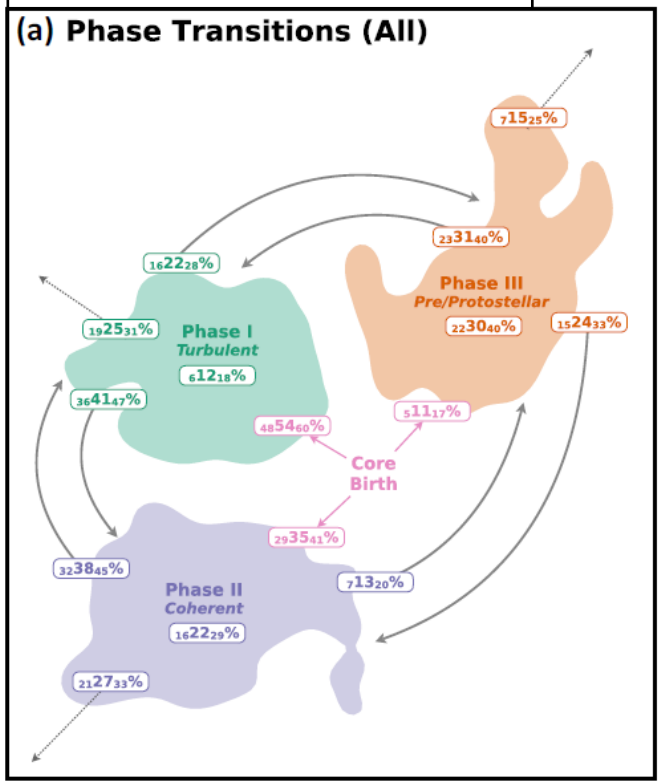

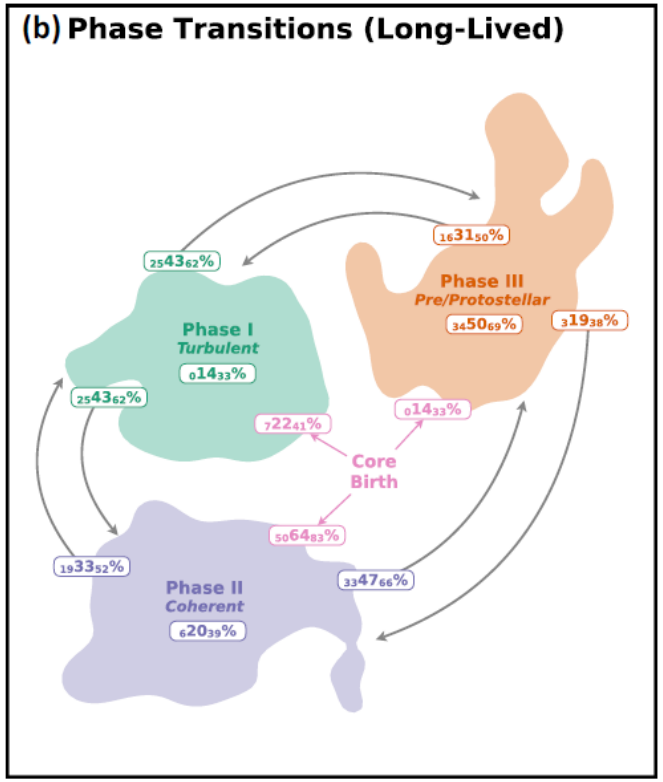

観測との比較

- 観測されたコアの性質を基にUMAP上に載せる

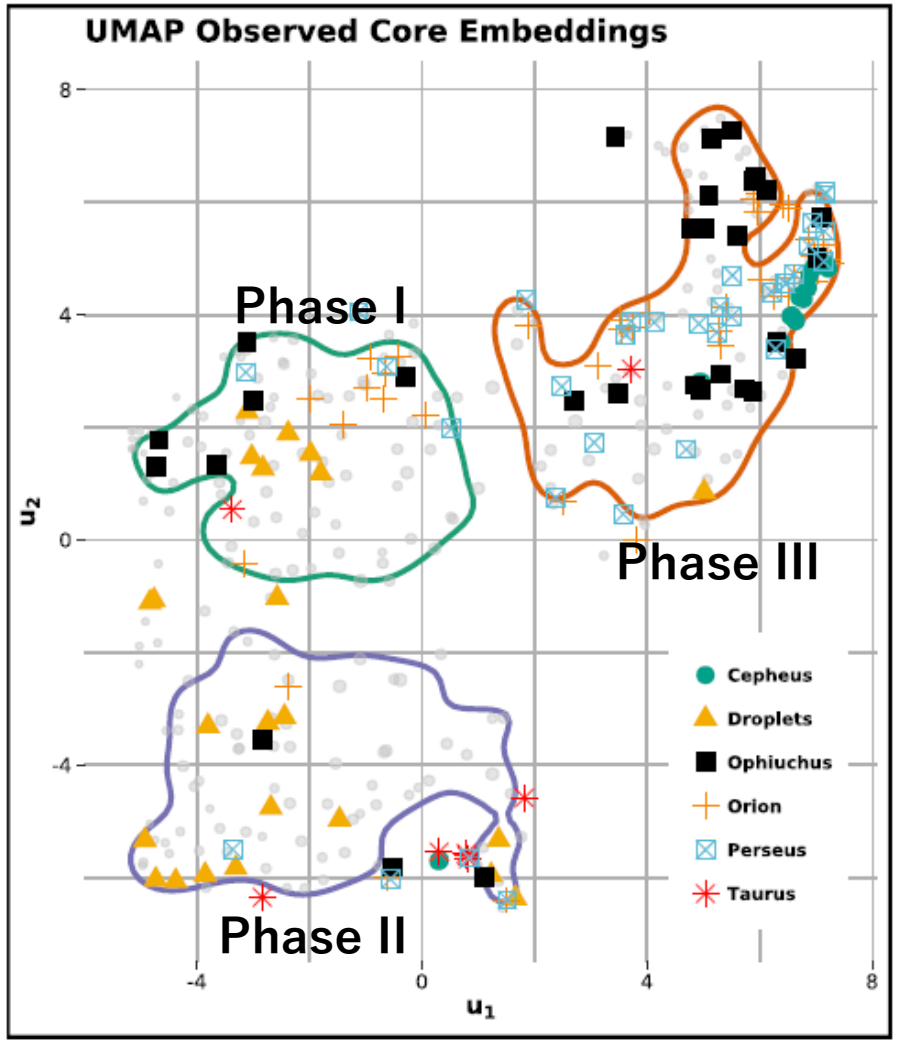

- 観測されたコアは総じて、３つのphaseに分布
- Droplet (Chen+2019)はほとんどPhase IIにある
  - Phase Iにもあるけど…
- Taurus分子雲ではPhase IIに存在
- Perseus, Ophiuchus, Orion分子雲では、Phase IIが少なくPhase IとIIIに多く分布
- Cepheusでは、Prestellarに対応する部分に分布

MHDシミュレーションから予想される確率的コアの運命

Table 2. Predicted future evolution for cores observed in each star-forming region. The table reports the number of observations from each region predicted to be in each evolutionary state along with the mean ±95 per cent confidence interval of the class-wise predictive probabilities.

		Disperse		Persist		Pre/Protostellar	
Region	*N*(total)	*N*	per cent	*N*	per cent	*N*	per cent
Ophiuchus	30	6	21 ± 9	4	21 ± 9	20	58 ± 14
Orion	43	3	19 ± 5	14	26 ± 8	26	55 ± 12
Cepheus	22	0	7 ± 2	2	13 ± 10	20	80 ± 10
Perseus	33	2	17 ± 6	12	31 ± 11	19	52 ± 13
Droplets	23	18	54 ± 12	4	39 ± 11	1	7 ± 7
Taurus	8	2	21 ± 27	6	65 ± 24	0	14 ± 8
All	159	31	22 ± 4	42	28 ± 4	86	50 ± 6

まとめ

- ３つの段階を同定
  - Phase I (turbulent), Phase II (coherent), Phase III (protostellar)
- コアの進化は、スナップショットでの性質では決まらない。
  - どのphaseも散逸する可能性がある。
  - Short lived coresはPhase IとPhase IIに存在
  - Long-lived coresはどのphaseにも存在し、phase間を移り変わる。
  - 原始星を作ったコアの元はどのphaseでも生まれ得るが、ほとんどの時間をPhase IIIで過ごす。
- 疑問
  - 現実の構造との関係があまり議論されていなかった。
  - coherent coreがどうやって維持されているのかよくわからなかった。

41. ## Backscattering and Line Broadening in Orion

C. R. O'Dell, G. J. Ferland, J. E. Mendez-Delgado ★ Examination of emission lines in high-velocity resolution optical spectra of the Orion Nebula confirms that the velocity component on the red wing of the main ionization front emission line is due to backscattering in the Photon Dominated Region. This scattered light component has a weak wavelength dependence that is consistent with either general interstellar medium particles or particles in the foreground of the Orion Nebula Cluster. An anomalous line-broadening component that has been known for 60+ years is characterized in unprecedented detail. Although this extra broadening may be due to turbulence along the line-of-sight of our spectra, we explore the possibility that it is due to Alvén waves in conditions where the ratio of magnetic and thermal energies are about equal and constant throughout the ionized gas.

42. # A Circumplanetary Dust Ring May Explain the Extreme Spectral Slope of the 10 Myr Young Exoplanet K2-33b

Kazumasa Ohno, Pa Chia Thao, Andrew W. Mann, Jonathan J. Fortney ★ Young exoplanets are attractive targets for atmospheric characterization to explore the early phase of planetary evolution and the surrounding environment. Recent observations of the 10 Myr young Neptune-sized exoplanet K2-33b revealed that the planet's transit depth drastically decreases from the optical to near-infrared wavelengths. Thao et al. (2022) suggested that a thick planetary haze and/or stellar spots may be the cause; however, even the best-fit model only barely explains the data. Here, we propose that the peculiar transmission spectrum may indicate that K2-33b possess a circumplanetary dust ring, an analog of Jupiter's dust ring. We demonstrate that the ring could produce a steep slope in the transmission spectrum even if its optical depth is as low as $\sim 10^{-2}$. We then apply a novel joint atmosphere-ring retrieval to K2-33b and find that the ring scenario could well explain the observed spectrum for various possible ring compositions. Importantly, the dust ring also exhibits prominent absorption features of ring particles around $\sim$10 μm, whose shape and strength depend on the composition of the ring. Thus, future observations by JWST-MIRI would be able to test not only the ring hypothesis but also, if it indeed exists, to constrain the composition of the ring – providing a unique opportunity to explore the origins of the dust ring around its parent planet, soon after the planetary system's formation.

43. Peering into the Young Planetary System AB Pic. Atmosphere, Orbit, Obliquity & Second Planetary Candidate

P. Palma-Bifani, G. Chauvin, M. Bonnefoy, P. M. Rojo, S. Petrus, L. Rodet, M. Langlois, F. Allard, B. Charnay, C. Desgrange, D. Homeier, A. -M. Lagrange, J. -L. Beuzit, P. Baudoz, A. Boccaletti, A. Chomez, P. Delorme, S. Desidera, M. Feldt, C. Ginski, R. Gratton, A. -L. Maire, M. Meyer, M. Samland, I. Snellen, A. Vigan, Y. Zhang

★ We aim to revisit the system AB Pic which has a known companion at the exoplanet/ brown-dwarf boundary. We based this study on a rich set of observations to investigate the companion's orbit and atmosphere. We composed a spectrum of AB Pic b merging archival VLT/SINFONI K-band data, with published spectra at J and H-band (SINFONI) and Lp-band (Magellan-AO), and photometric measurements (HST and Spitzer). We modeled the spectrum with ForMoSA, based on two atmospheric models: ExoREM and BT-SETTL13. We determined the orbital properties of b fitting the astrometric measurements from NaCo (2003 and 2004) and SPHERE (2015). The orbital solutions favor a semi-major axis of ∼190au viewed edge-on. With Exo-REM, we derive a T_{eff} of 1700±50K and surface gravity of 4.5±0.3dex, consistent with previous works, and we report for the first time a C/O ratio of 0.58±0.08 (∼solar). The posteriors are sensitive to the wavelength interval and the family of models used. Given the 2.1hr rotation period and our vsin(i) of ∼73km/s, we estimate for the first time the true obliquity to be ∼45 or ∼135deg, indicating a significant misalignment between the planet's spin and orbit orientations. Finally, the existence of a proper motion anomaly between the Hipparcos and Gaia eDR3 compared to our SPHERE detection limits and adapted radial velocity limits indicate the existence of a ∼6M_{Jup} inner planet orbiting from 2 to 10au (40-200mas). The possible existence of an inner companion, together with the likely miss-alignment of the spin axis orientation, strongly favor a formation path by gravitational instability or core accretion within a disk closer inside followed by dynamical interactions. Confirmation and characterization of planet c and access to a broader wavelength coverage for planet b will be essential to probe the uncertainties associated with the parameters.

44. ## Photometric and spectroscopic study of the EXor-like eruptive young star Gaia19fct

Sunkyung Park, Ágnes Kóspál, Péter Ábrahám, Fernando Cruz-Sáenz de Miera, Eleonora Fiorellino, Michał Siwak, Zsófia Nagy, Teresa Giannini, Roberta Carini, Zsófia Marianna Szabó, Jeong-Eun Lee, Jae-Joon Lee, Fabrizio Vitali, Mária Kun, Borbála Cseh, Máté Krezinger, Levente Kriskovics, András Ordasi, András Pál, Róbert Szakáts, Krisztián Vida, József Vinkó

★ Gaia19fct is one of the Gaia-alerted eruptive young stars that has undergone several brightening events. We conducted monitoring observations using multi-filter optical and near-infrared photometry, as well as near-infrared spectroscopy, to understand the physical properties of Gaia19fct and investigate whether it fits into the historically defined two classes. We present the analyses of light curves, color variations, spectral lines, and CO modeling. The light curves show at least five brightening events since 2015, and the multi-filter color evolutions are mostly gray. The gray evolution indicates that bursts are triggered by mechanisms other than extinction. Our near-infrared spectra exhibit both absorption and emission lines and show time-variability throughout our observations. We found lower rotational velocity and lower temperature from the near-infrared atomic absorption lines than from the optical lines, suggesting that Gaia19fct has a Keplerian rotating disk. The CO overtone features show a superposition of absorption and emission components, which is unlike other young stellar objects. We modeled the CO lines, and the result suggests that the emission and absorption components are formed in different regions. We found that although Gaia19fct exhibits characteristics of both types of eruptive young stars, FU Orionis-type objects (FUors) and EX Lupi-type objects (EXors), it shows more similarity with EXors in general.

45. **Three-dimensional evolution of radiative circumbinary discs: the size and shape of the inner cavity**

Arnaud Pierens, Richard Nelson ★ The evolution of circumbinary discs and planets is often studied using two-dimensional (2D) numerical simulations, although recent work suggests that 3D effects may significantly alter the structure of the inner cavity created by the binary. In this study, we present the results of 3D hydrodynamical simulations of circumbinary discs that orbit around analogues of the Kepler-16 and Kepler-34 systems, including the effect of stellar heating and radiative cooling on the thermal disc structure. We find that compared to their 2D counterparts, the structures of the cavities in 3D circumbinary disc models appear to reach a quasi-stationary state more rapidly, and in a subset of our runs the evidence for this is unambiguous. Furthermore, the sizes and eccentricities of the inner cavity are smaller in 3D compared to 2D. We attribute this difference to enhanced spiral wave dissipation in disc regions above the midplane, where the cooling time is of the order of the dynamical timescale, resulting in smaller inner cavity sizes in 3D disc models. Our results suggest that migrating planets should park closer to the central binary in 3D models of circumbinary discs, and point to the importance of including the 3D structure when simulating circumbinary discs and planets.

背景

- これまで15個のcircumbinary planetが発見されている。
- 15個のうち10個が、dynamical instability zone(連星による摂動で惑星がそとにはじき出される)のすぐ外に惑星が存在
  - シミュレーションにより、このような領域ではその場での惑星形成は難しいという示唆。
    さらに乱流を駆動するparameteric instabilityも起こることが示唆され、
    これもその場での惑星形成に影響する。
- 一方、周連星円盤の外側で惑星を作り、内側に移動してきたことも考えられる。

周連星円盤における惑星移動 (背景)

周連星円盤でできた惑星は、周連星円盤の内縁へ向かって移動する

- 連星の離心率がmoderateな場合
  - 内縁で、正の共回転トルクが働くため移動が止まる (Masse+2006,Penzin+2021など)。
- 連星が大きな離心率を持っている場合
  - 周連星円盤も大き離心率を持ち、それにより惑星も大きな離心率を獲得。
  - それにより中心連星よりも離れた場所で惑星移動がとまり、観測を説明できない。
  - 最近の研究(Mutter+2017, Penzin+2021)では、惑星がギャップを開けるほど十分重ければ、inner cavityを円にできて、惑星がより中心まで移動できる可能性を示唆

これまでの2次元計算に限られていたことから、この論文で現実的な３次元計算をおこない、惑星移動過程を調べる。

セットアップ

- 3次元計算：エネルギー方程式に冷却を入れる。
  - Tirrはradmc3d計算で決める(0.1um～10umでMRN分布)。100時間ステップごとにTirrを更新

$$Q_{\rm cool} = -\rho c_v \frac{T - T_{\rm irr}}{t_{\rm cool}}, \qquad t_{\rm cool} = \frac{\rho c_v H \tau_{\rm eff}}{3\sigma T^3}, \qquad \tau_{\rm eff} = \frac{3}{8}\tau + \frac{\sqrt{3}}{4} + \frac{1}{4\tau}.$$

上からと下から測定した光学的厚みの調和平均

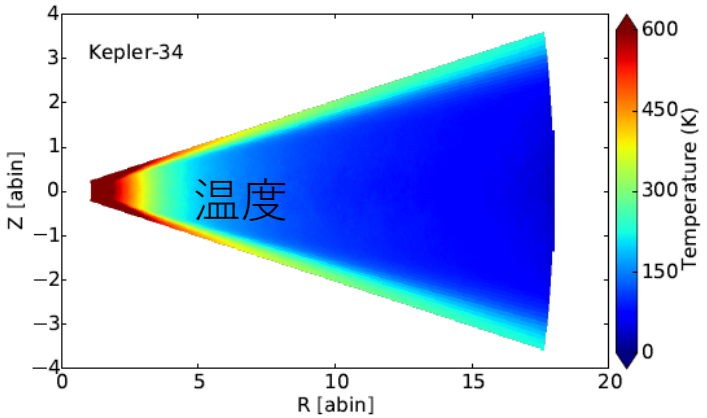

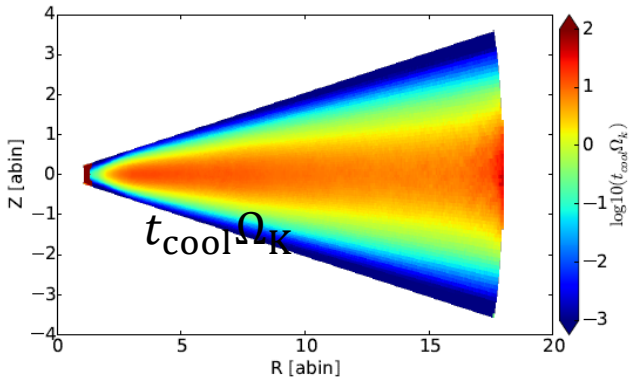

- 2次元計算も行う。その場合 $\tau = \frac{c_1}{\sqrt{2\pi}}\kappa\Sigma.$

System	$M_1(M_\odot)$	$M_2(M_\odot)$	$R_1(R_\odot)$	$R_2(R_\odot)$	$T_1(K)$	$T_2(K)$	$a_{\rm bin}$ (AU)	$e_{\rm bin}$
Kepler-16	0.69	0.20	0.65	0.23	4450	3311	0.22	0.16
Kepler-34	1.05	1.02	1.16	1.09	5913	5867	0.23	0.54

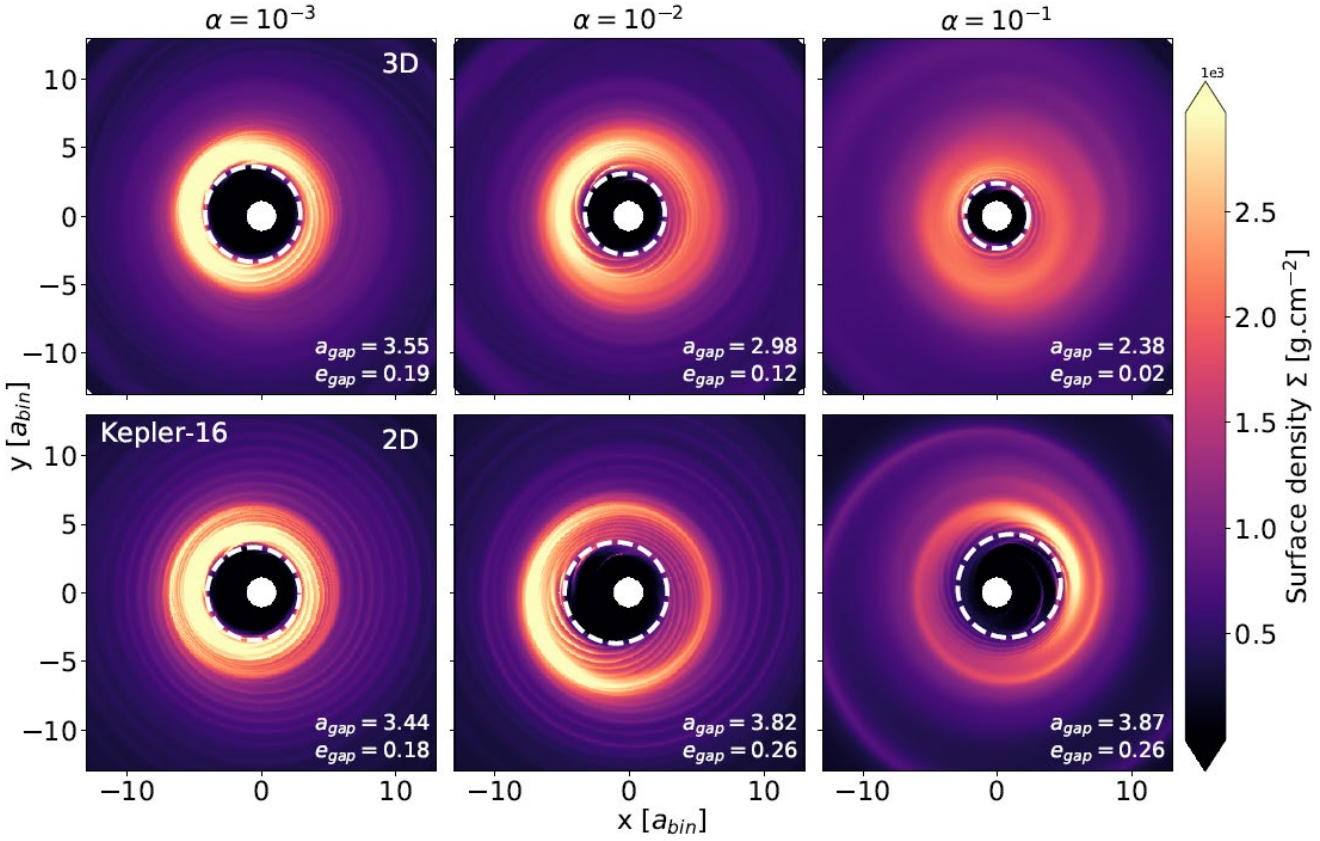

- $\alpha = 10^{-3}$の場合
  - 2Dと3Dは非常に似ている
- $\alpha = 10^{-2}$ and 0.1の場合
  - 3Dの方がinner cavityの半径が小さく、離心率が小さい。

2次元と3次元の違い

- Inner cavitiyは、中心連星が立てるspiral waveによって角運動量が円盤に輸送されることでできる。
- Spiral waveは、冷却時間がisothermal limit $t_{\mathbf{cool}} \ll \Omega^{-1}$から増加すると弱まり、$t_{\mathbf{cool}} \sim \Omega^{-1}$を超えると、adiabatic limitに近づき、spiral waveはまた強くなる。
  - 2D計算では、$\beta \sim 10$ で、断熱的にふるまいspiral waveが強い
  - 3D計算では、赤道面付近で$\beta \sim 100$となり、円盤表面で$\beta \sim 10^{-3}$となる。→ 中間的な高度ではspiral waveを減衰させる。
  - αによるふるまいの違いは？

46. # Accretion process, magnetic fields, and apsidal motion in the pre-main sequence binary DQ Tau

Kim Pouilly, Oleg Kochukhov, Ágnes Kóspál, Axel Hahlin, Andres Carmona, Péter Ábrahám ★

Classical T Tauri stars (CTTSs) are young stellar objects that accrete materials from their accretion disc influenced by their strong magnetic field. The magnetic pressure truncates the disc at a few stellar radii and forces the material to leave the disc plane and fall onto the stellar surface by following the magnetic field lines. However, this global scheme may be disturbed by the presence of a companion interacting gravitationally with the accreting component. This work is aiming to study the accretion and the magnetic field of the tight eccentric binary DQ Tau, composed of two equal-mass (~ 0.6 $M_{\odot}$) CTTSs interacting at different orbital phases. We investigated the variability of the system using a high-resolution spectroscopic and spectropolarimetric monitoring performed with ESPaDOnS at the CFHT. We provide the first ever magnetic field analysis of this system, the Zeeman-Doppler imaging revealed a stronger magnetic field for the secondary than the primary (1.2 kG and 0.5 kG, respectively), but the small-scale fields analysed through Zeeman intensification yielded similar strengths (about 2.5 kG). The magnetic field topology and strengths are compatible with the accretion processes on CTTSs. Both components of this system are accreting, with a change of the main accretor during the orbital motion. In addition, the system displays a strong enhancement of the mass accretion rate at periastron and apastron. We also discovered, for the first time in this system, the apsidal motion of the orbital ellipse.

47. Differences in chemical evolution between isolated and embedded prestellar cores

F. D. Priestley, A. P. Whitworth, E. Fogerty ★ Models of prestellar cores often assume that the cores are isolated from their environment - material outside the core boundary plays no role in the subsequent evolution. This is unlikely to be the case in reality, where cores are located within hierarchically substructured molecular clouds. We investigate the dynamical and chemical evolution of prestellar cores, modelled as Bonnor-Ebert spheres, and show that the density of the ambient medium has a large impact on the resulting chemical properties of the cores. Models embedded in high-density, low-temperature surroundings have greatly enhanced abundances of several molecules, such as CO and CS, compared to models with more diffuse surroundings, corresponding to relatively isolated cores. The predicted intensities and profile shapes of molecular lines are also affected. The density of the ambient medium has a stronger effect on the chemical evolution than whether the cores are initially in or out of equilibrium. This suggests that the impact of environment cannot be neglected when modelling chemistry in prestellar cores; the results of these models are highly sensitive to the assumptions made about the core surroundings.

48. A Massive Star is Born: How Feedback from Stellar Winds, Radiation Pressure, and Collimated Outflows Limits Accretion onto Massive Stars

Anna L. Rosen ★
Massive protostars attain high luminosities as they are actively accreting and the radiation pressure exerted on the gas in the star's atmosphere may launch isotropic high-velocity winds. These winds will collide with the surrounding gas producing shock-heated ($T \sim 10^7$ K) tenuous gas that adiabatically expands and pushes on the dense gas that may otherwise be accreted. We present a suite of 3D radiation-magnetohydrodynamic simulations of the collapse of massive prestellar cores and include radiative feedback from the stellar and dust-reprocessed radiation fields, collimated outflows, and, for the first time, isotropic stellar winds to model how these processes affect the formation of massive stars. We find that winds are initially launched when the massive protostar is still accreting and its wind properties evolve as the protostar contracts to the main-sequence. Wind feedback drives asymmetric adiabatic wind bubbles that have a bipolar morphology because the dense circumstellar material pinches the expansion of the hot shock-heated gas. We term this the "wind tunnel effect." If the core is magnetized, wind feedback is less efficient at driving adiabatic wind bubbles initially because magnetic tension delays their growth. We find that wind feedback eventually quenches accretion onto $\sim$30 $M_\odot$ protostars that form from the collapse of the isolated cores simulated here. Hence, our results suggest that $\gtrsim$30 $M_\odot$ stars likely require larger-scale dynamical inflows from their host cloud to overcome wind feedback. Additionally, we discuss the implications of observing adiabatic wind bubbles with

49. The core population and kinematics of a massive clump at early stages: an ALMA view

E. Redaelli, S. Bovino, P. Sanhueza, K. Morii, G. Sabatini, P. Caselli, A. Giannetti, S. Li ★

High-mass star formation theories make distinct predictions on the properties of the prestellar seeds of high-mass stars. Observations of the early stages of high-mass star formation can provide crucial constraints, but they are challenging and scarce. We investigate the properties of the prestellar core population embedded in the high-mass clump AGAL014.492-00.139, and we study the kinematics at the clump and the clump-to-core scales. We have analysed an extensive dataset acquired with the ALMA interferometer. Applying a dendrogram analysis to the Band o-H_2D^+ data, we identified 22 cores. We have fitted their average spectra in local-thermodinamic-equilibrium conditions, and we analysed their continuum emission at 0.8 mm. The cores have transonic to mildly supersonic turbulence levels and appear mostly low-mass, with $M_{\rm core} < 30\,{\rm M}_\odot$. Furthermore, we have analysed Band 3 observations of the N_2H^+ (1-0) transition, which traces the large scale gas kinematics. Using a friend-of-friend algorithm, we identify four main velocity coherent structures, all of which are associated with prestellar and protostellar cores. One of them presents a filament-like structure, and our observations could be consistent with mass accretion towards one of the protostars. In this case, we estimate a mass accretion rate of $\dot{M}_{\rm acc} \approx 2 \times 10^{-4}\,{\rm M}_\odot\,{\rm yr}^{-1}$. Our results support a clump-fed accretion scenario in the targeted source. The cores in prestellar stage are essentially low-mass, and they appear subvirial and gravitationally bound, unless further support is available for instance due to magnetic fields.

50. # A large (1 pc) contracting envelope around the prestellar core L1544

E. Redaelli, A. Chacón-Tanarro, P. Caselli, M. Tafalla, J. E. Pineda, S. Spezzano, O. Sipilä ★

Prestellar cores, the birthplace of Sun-like stars, form from the fragmentation of the filamentary structure that composes molecular clouds, from which they must inherit at least partially the kinematics. Furthermore, when they are on the verge of gravitational collapse, they show signs of subsonic infall motions. How extended these motions are, which depends on how the collapse occurs, remains largely unknown. We want to investigate the kinematics of the envelope that surrounds the prototypical prestellar core L1544, studying the cloud-core connection. To our aims, we observed the HCO^+(1-0) transition in a large map. HCO+ is expected to be abundant in the envelope, making it an ideal probe of the large-scale kinematics in the source. We modelled the spectrum at the dust peak by means of a non local-thermodynamical-equilibrium radiative transfer. In order to reproduce the spectrum at the dust peak, a large ($\sim 1\,$pc) envelope is needed, with low density (tens of cm^{-3} at most) and contraction motions, with an inward velocity of $\approx 0.05\,km\,s^{-1}$. We fitted the data cube using the Hill5 model, which implements a simple model for the optical depth and excitation temperature profiles along the line-of-sight, in order to obtain a map of the infall velocity. This shows that the infall motions are extended, with typical values in the range $0.1 - 0.2\,km\,s^{-1}$. Our results suggest that the contraction motions extend in the diffuse envelope surrounding the core, which is consistent with recent magnetic field measurements in the source, which showed that the envelope is magnetically supercritical.

51. ## Interpreting molecular hydrogen and atomic oxygen line emission of T Tauri disks with photoevaporative disk-wind models

Ch. Rab, M. Weber, T. Grassi, B. Ercolano, G. Picogna, P. Caselli, W. -F. Thi, I. Kamp, P. Woitke ★

Winds in protoplanetary disks play an important role in their evolution and dispersal. However, what physical process is driving the winds is still unclear (i.e. magnetically vs thermally driven), and can only be understood by directly confronting theoretical models with observational data. We use hydrodynamic photoevaporative disk-wind models and post-process them with a thermo-chemical model to produce synthetic observables for the o-H_2 at 2.12 micron and [OI] at 0.63 micron spectral lines and directly compare the results to a sample of observations. Our photoevaporative disk-wind model is consistent with the observed signatures of the blueshifted narrow low-velocity component (NLVC), which is usually associated with slow disk winds, for both tracers. Only for one out of seven targets that show blueshifted NLVCs does the photoevaporative model fail to explain the observed line kinematics. Our results also indicate that interpreting spectral line profiles by simple methods, such as the thin-disk approximation, to determine the line emitting region can yield misleading conclusions. The photoevaporative disk-wind models are largely consistent with the studied observational data set, but it is not possible to clearly discriminate between different wind-driving mechanisms. Further improvements to the models, such as consistent modelling of the dynamics and chemistry and detailed modelling of individual targets would be beneficial. Furthermore, a direct comparison of magnetically driven disk-wind models to the observational data set is necessary in order to determine whether or not spatially unresolved observations of multiple wind tracers are sufficient to discriminate between theoretical models.

52. # Stellar Properties for a Comprehensive Collection of Star Forming Regions in the SDSS APOGEE-2 Survey

Carlos G. Román-Zúñiga, Marina Kounkel, Jesús Hernández, Karla Peña Ramírez, Ricardo López-Valdivia, Kevin R. Covey, Amelia M. Stutz, Alexandre Román-López, Hunter Campbell, Eliott Khilfeh, Mauricio Tapia, Guy S. Stringfellow, Juan José Downes, Keivan G. Stassun, Dante Minniti, Amelia Bayo, Jinyoung Serena Kim, Genaro Suárez, Jason Ybarra, José G. Fernández-Trincado, Penélope Longa-Peña, Valeria Ramírez-Preciado, Javier Serna, Richard R. Lane, D. A. García-Hernández, Rachael L. Beaton, Dmitry Bizyaev, Kaike Pan ★

The Sloan Digital Sky Survey IV (SDSS-IV) APOGEE-2 primary science goal was to observe red giant stars throughout the Galaxy to study its dynamics, morphology, and chemical evolution. The APOGEE instrument, a high-resolution 300 fiber H-band (1.55-1.71 micron) spectrograph, is also ideal to study other stellar populations in the Galaxy, among which are a number of star forming regions and young open clusters. We present the results of the determination of six stellar properties (T_{eff}, $\log g$, [Fe/H], $L/L_{\odot}$, $M/M_{\odot}$, and ages) for a sample that is composed of 3360 young stars, of sub-solar to super-solar types, in sixteen Galactic star formation and young open cluster regions. Those sources were selected by using a clustering method that removes most of the field contamination. Samples were also refined by removing targets affected by various systematic effects of the parameter determination. The final samples are presented in a comprehensive catalog that includes all six estimated parameters. This overview study also includes parameter spatial distribution maps for all regions and Hertzprung-Russell ($L/L_{\odot}$ vs. T_{eff}) diagrams. This study serves as a guide for detailed studies on individual regions, and paves the way for the future studies on the global properties of stars in the pre-main sequence phase of stellar evolution using more robust samples.

53. Accretion variability in RU Lup

Camille Stock, Pauline McGinnis, Alessio Caratti o Garatti, Antonella Natta, Tom P. Ray ★ The process of accretion in classical T Tauri stars (CTTSs) has been observed to vary on different timescales. Studying this variability is vital to understanding a star's evolution and provides insight into the complex processes at work within. Understanding the dichotomy between continuum veiling and emission line veiling is integral to accurately measuring the amount of veiling present in stellar spectra. Here, 15 roughly consecutive nights of optical spectroscopic data from the spectropolarimeter ESPaDOnS are utilised to characterise the short-term accretion activity in the CTTS, RU Lup, and investigate its relationship with the veiling in the LiI 6707A absorption line. The accretion-tracing HI Balmer series emission lines were studied and used to obtain the accretion luminosity (Lacc) and mass accretion rate (Macc) for each night, which vary by a factor of 2 between the brightest and dimmest nights. We also measured the veiling using multiple photospheric absorption lines (NaI 5688A, MnI 6021A, and LiI 6707A) for each night. We find the LiI 6707A line provides measurements of veiling that produce a strong, positive correlation with Lacc in the star. When corrected for Li depletion, the average veiling measured in the LiI 6707A line is $r_{LiI(avg)}$ ∼3.25±0.20, which is consistent with the other photospheric lines studied (r_avg ∼3.28±0.65). We measured short timescale variability in the Lacc and Macc that are intrinsic and not due to geometric effects. Upon comparing the changes in veiling and Lacc, we find a strong, positive correlation. This study provides an example of how this correlation can be used as a tool to determine whether a measured variability is due to extinction or an intrinsic change in accretion. As the determination of veiling is an independent process from measuring Lacc, their relationship allows further exploration of accretion phenomena in young stars.

54. High-contrast Imaging around a 2 Myr-old CI Tau with a Close-in Gas Giant

Toshinori Shimizu, Taichi Uyama, Yasunori Hori, Motohide Tamura, Nicole Wallack ★ Giant planets around young stars serve as a clue to unveiling their formation history and orbital evolution. CI Tau is a 2 Myr-old classical T-Tauri star hosting an eccentric hot Jupiter, CI Tau b. The standard formation scenario of a hot Jupiter predicts that planets formed further out and migrated inward. A high eccentricity of CI Tau b may be suggestive of high-e migration due to secular gravitational perturbations by an outer companion. Also, ALMA 1.3 mm-continuum observations show that CI Tau has at least three annular gaps in which unseen planets may exist. We present high-contrast imaging around CI Tau taken from Keck/NIRC2 L'-band filter and vortex coronagraph that allows us to search for an outer companion. We did not detect any outer companion around CI Tau from angular differential imaging (ADI) using two deep imaging data sets. The detection limits from ADI-reduced images rule out the existence of an outer companion beyond ~ 30 au that can cause the Kozai-Lidov migration of CI Tau b. Our results suggest that CI Tau b may have experienced Type II migration from $\lesssim 2$ au in Myrs. We also confirm that no planets with $\geq 2-4\,M_{\rm Jup}$ are hidden in two outer gaps.